Langmuir

ARTICLE

pubs.acs.org/Langmuir

Manipulation of Cracks in Three-Dimensional Colloidal Crystal Films via Recognition of Surface Energy Patterns: An Approach to Regulating Crack Patterns and Shaping Microcrystals

Wei Sun,[†] Fei Jia,[†] Zhiqiang Sun,[‡] Junhu Zhang,[*,†] Yang Li,[†] Xun Zhang,[†] and Bai Yang[†]

[†]State Key Laboratory of Supramolecular Structure and Materials, College of Chemistry, Jilin University, Changchun 130012, PR China

[‡]Changchun Institute of Applied Chemistry, Chinese Academy of Sciences, Changchun 130022, PR China

Supporting Information

ABSTRACT: A new concept for dealing with cracks in colloidal crystals has been proposed. We induce the cracks rather than eliminate them via templates that possess hydrophilic/hydrophobic patterns on the surface (surface energy patterns), leading the cracks to propagate along the predetermined lines. Colloidal crystal arrays with various kinds of element figures separated by cracks could be reproducibly fabricated. Diverse crack patterns other than common stripes have been observed, and the mechanism of these behaviors has been explored. The factors that influence the crack density have been investigated to ensure that the templates could function effectively. Moreover, we obtained microcrystal blocks with specific shapes, detached from the substrate.

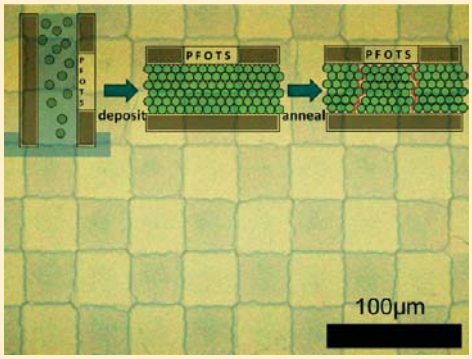

INTRODUCTION

Though it has been decades since colloidal crystals (CCs) were proven to be promising for producing photonic crystals,[1] the strong interest in this kind of versatile material has never faded away.[2,3] Because various methods have already been well established for constructing large-area opals with controllable thickness[4] and bandgap,[5] other aspects deserving investigation started to engage people's attention, such as patterning techniques that intend to achieve photonic device integration,[6,7] methods to obtain single crystals used as supports for assays,[8] the fabrication of anisotropic CCs,[9] a self-assembly mechanism[10] as well as the observation of dissipative patterns,[11] and the realization of CCs' applications as substrates for surface-enhanced Raman scattering (SERS),[12,13] templates for fabricating macroporous structures[14,15] or nanostructure arrays,[16,17] and amplifiers to enhance emissions.[18,19]

With respect to these aspects, researchers are facing mainly two problems. First, facile methods are still needed to ensure that the colloidal spheres could exactly assemble into predetermined places, exhibiting certain crystal shapes. Second, the formation of irregular cracks and other random defects remains a plague. To our knowledge, few publications have been devoted to dealing with both problems together because preventing the nucleation of cracks seemed irrelevant to patterning the colloidal crystals into designed geometries.

Much interest has been focused on the microcracks that arose upon drying because of the shrinkage of the colloidal spheres. In some methods, people tried to eliminate the cracks by sticking the spheres together before they shrank[20,21] and succeeded in obtaining large-area opal structures, but the resulting products still included impurities, which might somehow make the synthesis of inverse opal difficult. Other groups have observed crack patterns in the course of drying the colloidal suspensions[22] and further described the fracture mechanisms to help understand the cracking behaviors,[23,24] but the pity is that the patterns were mainly stripes with regular widths, lacking other figures. To truly manipulate the cracks more than just to understand them, we deal with the cracks in a different way (i.e., we introduce them into certain regions rather than eliminating them). Because the lateral shrinkage is demonstrated to be severely affected by the support,[25] we used patterned substrates to generate a discrepancy during shrinkage, thus manipulating the paths of the propagating cracks.

In this article, we report a new method by which we could manipulate the cracks to propagate along the predetermined lines, and at the same time these cracks cleaved the colloidal crystal films into cakelike single crystals with demanded shapes and micrometer-scale sizes. A simple method was used wherein we employed physical confinement and a prepatterned substrate surface displaying variations in interfacial energies. The self-assembly process was achieved by evaporating the solvent from a colloidal suspension between hydrophilic glass and a patterned Si

Received: January 18, 2011
Revised: April 12, 2011
Published: June 01, 2011

substrate, following our reported work.[26] Three-dimensional colloidal crystal films were formed with the protection of the two substrates, thus exhibiting high stability with respect to the solvent and environment. Usually, as soon as the colloidal spheres have assembled into an fcc (face-centered cubic) lattice, the colloidal crystal will undergo uniform shrinkage to form the final cracked morphology.[27] However, the patterned Si substrate would bring about a discrepancy during the shrinkage process. Finally, the stress would be preferentially relieved at the borderlines of the two kinds of elements, causing the cracks to propagate along the hydrophilic/hydrophobic boundaries.

EXPERIMENTAL SECTION

Materials. We demonstrated the approach using two kinds of silica spheres with different diameters (230 and 260 nm) synthesized by a modified procedure originally described by Stöber et al.[28] The spheres were dispersed in ethanol and preserved in airtight bottles. The silicon wafers for the fabrication of templates and glass substrates for the deposition of silica spheres were all cautiously pretreated with piranha solution (a boiling mixture of 98% H_2SO_4 and 30% H_2O_2 in a volumetric ratio of 7:3, a strong oxide) for 20 min to increase the hydrophilicity of the surface and then rinsed with deionized water. 1*H*,1*H*,2*H*,2*H*-Perfluorooctyltrichlorosilane ($C_8H_4C_{l3}F_{13}Si$, PFOTS) was purchased from Sigma-Aldrich and used as received. PVP (poly(vinylpyrrolidone), MW 0.36 million) was dissolved in water to make a 10 mg/mL solution.

Fabrication of the Patterned Template Substrates. We began with a photolithography process to cover the Si wafers with various photoresist patterns. After the development procedure, the periodic figures of the photoresist were left on the surface, with the residual surface regions uncovered in exactly the same manner as for the patterns on the photomasks that we designed (photoresist patterns in Supporting Information, Figure S1). Subsequently, a vapor deposition process of PFOTS was applied to these substrates to assemble the molecules on whole surfaces. Specifically, 50 μL of PFOTS and the substrates were heated together in an airtight jar at 80 °C for 0.5 h. Finally, we used ethanol associated with sonication for 10 min to clean off the photoresist together with the PFOTS on it, leaving the hydrophobic molecules only on the originally bared surface regions. Thus, a surface energy pattern was obtained, which retained the figures of the photoresist pattern.

Preparation of Spatially Patterned Colloidal Crystals and Manipulation of the Cracks. The subsequent self-assembly process used to form CCs follows a procedure combining capillarity and vertical deposition[26] (Figure 1). We vertically placed two square substrates (1 × 1 cm^2 or 1.5 × 1.5 cm^2) close together in the colloidal suspension (silica spheres dispersed in 1 mL of ethanol), leading to the suspension located between the two substrates due to capillarity. One of the substrates was the patterned Si wafer, which was first put in the container vertically with two edges contacting the inner wall; the other was a transparent glass substrate to allow us to observe the inner situation through it and moved to approach the patterned wafer in parallel. Once the suspension filled the space between the two substrates, the outside atmospheric pressure would press the substrates together and they would not easily break apart from each other. The thickness (measured from the SEM cross-sectional view) of the colloidal crystals varies with the initial microsphere concentration before the solvent evaporates. It typically took 3 to 4 days at room temperature for the deposition process if the suspension was put into a 10 mL cylinder glass container with ~25 holes punched through the polymer-film lid by a syringe needle (mean diameter of holes ~1 mm). In the control experiments performed to explain the formation mechanism of the crack patterns, 100 μL of 10 mg/mL PVP was added to a 1 mL colloidal suspension, leading the spheres to stick to each other more firmly during self-assembly and shrinkage. With regard to Pollack's

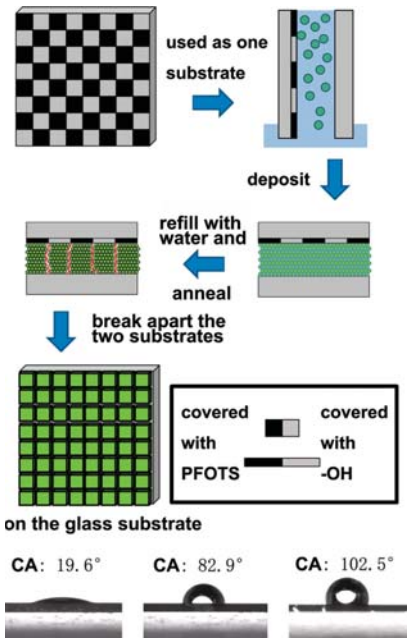

Figure 1. Schematic illustration of the two-substrate vertical deposition method and the manipulation process for cracks. The red lines represent cracks that penetrated the film, connecting the two substrates. The 3D colloidal crystal film is finally segmented by these cracks, forming small blocks that retain the designed shape (square in this illustration). The photographs below were water droplets (each 4 μL) on a hydrophilic Si wafer, a template substrate (square lattice pattern), and a fully PFOTS-modified Si wafer from left to right, respectively.

work,[29] the system was stored in a cabinet to avoid the influence of light and air flow. As soon as the dispersed ethanol completely evaporated under visual observation (although the spheres were still wet[30]) and the diffraction color occurred, an annealing process was applied to these unseparated sandwiches to allow the cracks to grow deeper and wider, penetrating the crystal film and splitting it into blocks with certain shapes by completely moisturizing the colloidal crystal with deionized water, followed by heating them in an oven at the temperature that we intentionally set (50−100 °C) for 3 h. In addition, the crack density was mainly adjusted by changing the appropriate film thicknesses as well taking into consideration the annealing temperature and the sphere size. After the sandwiches were cooled to room temperature, we opened them to observe the inner morphologies. The crack densities were measured and calculated according to the optical photographs (351 × 263 μm^2) following a method described elsewhere.[31]

Calcination. To obtain stable photonic device chips, the annealed samples were subsequently calcinated with a pipe furnace at 450 °C for 1 h and then at 700 °C for 2 h[5] to improve the mechanical strength. The samples were then cooled slowly in the pipe to room temperature. Fast cooling should be avoided to prevent the formation of extra cracks due to severe cold contraction. The single-crystal elements could be detached as microblocks by sticking them up from the substrate with a piece of tape.

Characterization. Scanning electron microscopy (SEM) images were recorded on a JEOL JSM6700F field emission scanning electron microscope with a primary electron energy of 3 kV. The samples of SEM were sputter coated with a Pt film prior to examination. The optical images were recorded on an Olympus BX51 microscope (in reflection mode) and were captured with an MVC1000 USB2.0 megapixel camera. The normal specular reflectance was measured by homemade equipment consisting of a collimated beam of a fiber-coupled tungsten−bromine

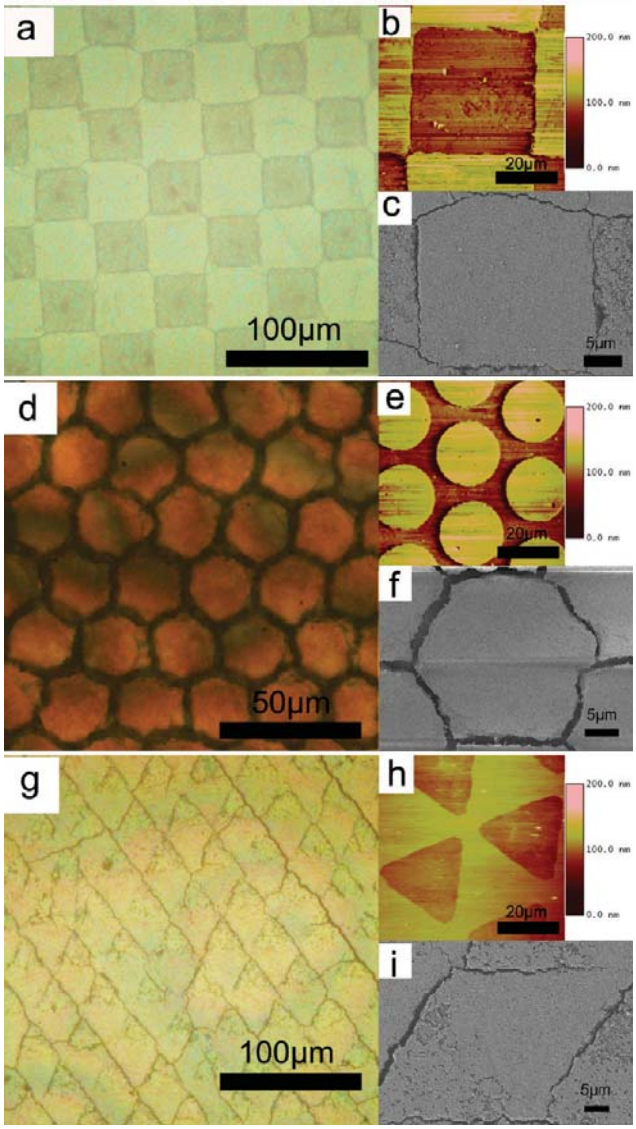

Figure 2. (a, d, g) Optical images of various patterns of cracks: square lattice (230 nm spheres, 7.89 μm), honeycomb (260 nm spheres, 9.24 μm, calcinated to increase the width of the cracks), and rhombus lattice (230 nm spheres, 5.50 μm), respectively. (b, e, h) AFM images of the corresponding template surfaces. (c, f, i) SEM images of CC units.

lamp (Ocean Optics), and the spectra were obtained using a spectrometer (Maya 2000 pro) from 400 to 800 nm. Atomic force microscopy (AFM) images of the surface energy patterns were measured with a Digital Instruments NanoScope IIIa in contact mode.

RESULTS AND DISCUSSION

Various Crack Patterns and CC Arrays Achieved by Template Recognition. As shown schematically in Figure 1, the template substrates with surface energy patterns in our method played a crucial role in regulating the cracking paths. The PFOTS treatment would surely turn the surface from hydrophilic to hydrophobic according to the contact angle measurements (from CA 19.6° to CA 102.5°), but the alternative hydrophilic/hydrophobic surface exhibited an overall state (CA 82.9°) that did not reach the transition state (CA 90°), which allowed the successful

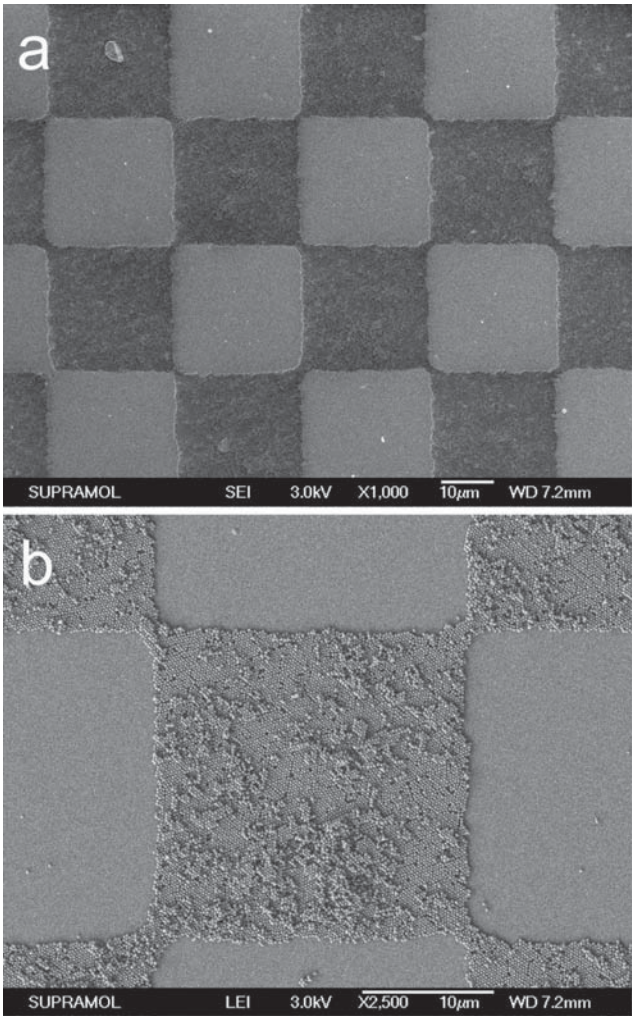

Figure 3. (a) SEM image of the resultant array structure on the template substrate (square lattice) after the two substrates were broken apart. (b) Enlarged SEM image showing the morphology of the surface.

deposition of the spheres from the suspension. The 3D CC films confined between the template substrate and the cover glass substrate were annealed after the deposition process. If the crack spacing (see details in the section Crack Density) matches the periodicity of the template pattern, then these cracks would cleave the entire colloidal crystal film into small single crystals with the shapes that we designed. In addition, during the breaking apart of sandwich, these CCs would preferentially attach to the cover glass substrate with very few spheres left on the template. We employed template substrates with different patterns to demonstrate this effect. Several kinds of CC arrays on the cover glass substrates segmented by the induced crack patterns are displayed in Figure 2a,d,g (square lattice, honeycomb, and rhombus lattice, respectively). The regulated cracks can be clearly observed with an optical microscope. In addition, few cracks can be found within the single crystals. The mechanism for the cracks to recognize the template pattern will be discussed later in this article. Moreover, besides this kind of crack pattern, another kind of brightness (roughness) pattern was observed. Figure 2a clearly reveals that the brightness differs periodically, forming a brightness pattern corresponding well to the template

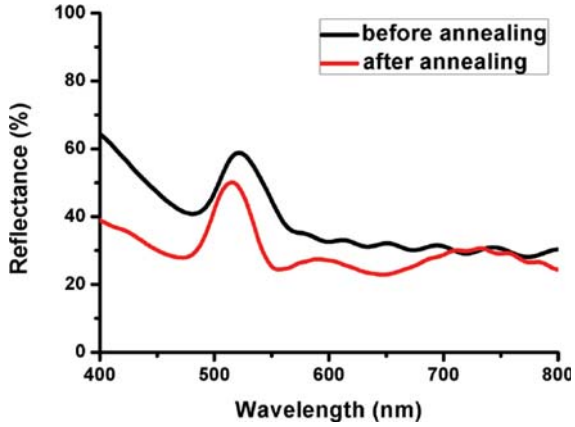

Figure 4. Reflection spectrum of the CC film before (black) and after (red) an anneal process (60 °C). The sphere size is ~230 nm measured with SEM. The peak wavelengths were 522 nm and 515 nm, respectively.

substrate. We conceive that this phenomenon originates from the periodic roughness of the CCs' surfaces. From the AFM images taken in contact mode in Figure 2b,e,h, it is easy to see the chemical contrast between the PFOTS-covered regions and the hydrophilic regions on the template substrate surfaces, which will further generate stickiness contrast as demonstrated by Parikh et al.[32] As a result, the surfaces of the CCs that were previously against the hydrophilic regions will become slightly rough (Figure 2c) after the sandwich is opened up because some spheres were left on the template (Figure 3); therefore, the rough surfaces will scatter the incident light and appear darker in reflection mode. However, the single crystals against both kinds of regions did not grow separately before the cracks formed, thus appearing uniform in both growth orientation and structure. (Another close-up image of the sphere packing on both sides of a linear crack is shown in Supporting Information Figure S2). Though the patterns are not very complex, we believe that this method would still operate for similar array patterns that are critical to photonic device integration. To confirm the optical property of the colloidal crystals array, we have measured the reflection spectra. Obvious peaks of the same square array sample (length 25 μm) before annealing and after annealing appeared in the spectrum shown in Figure 4. The sandwich was not opened in this case to compare the crystal quality. It seemed that the annealing process removed the small amount of remnant solvent and eliminated a few defects (not cracks), thus resulting in a narrower peak at a smaller wavelength with a lower background reflection. (The reflectance at the peak would be higher for the annealed sample if the background were subtracted.) For such a 3D photonic crystal, the diffraction wavelength of the photonic band gap obeys the derivative law[33] of Bragg's law

$$\lambda = 2d_{111}n_{\mathrm{eff}} = 2d_{111}\sqrt{n_{\mathrm{sp}}{}^2 f + n_{\mathrm{vo}}{}^2(1-\mathrm{f})\sin\theta}$$

where λ is the diffraction wavelength, n_{eff} is the effective refractive index, θ is the incident angle of light, $n_{\mathrm{sp}} = 1.45$ and $n_{\mathrm{vo}} = 1.0$ are refractive indexes of silica microspheres and air in the voids, respectively, and f is the filling ratio of silica spheres. For the fcc structure closely packed along the (111) face, $d_{111} = 0.816D$, in which D is the diameter of the spheres. Using this law to deduce the diffraction wavelength, the peak before annealing (522 nm) is more red-shifted than is the annealed one (515 nm) with respect

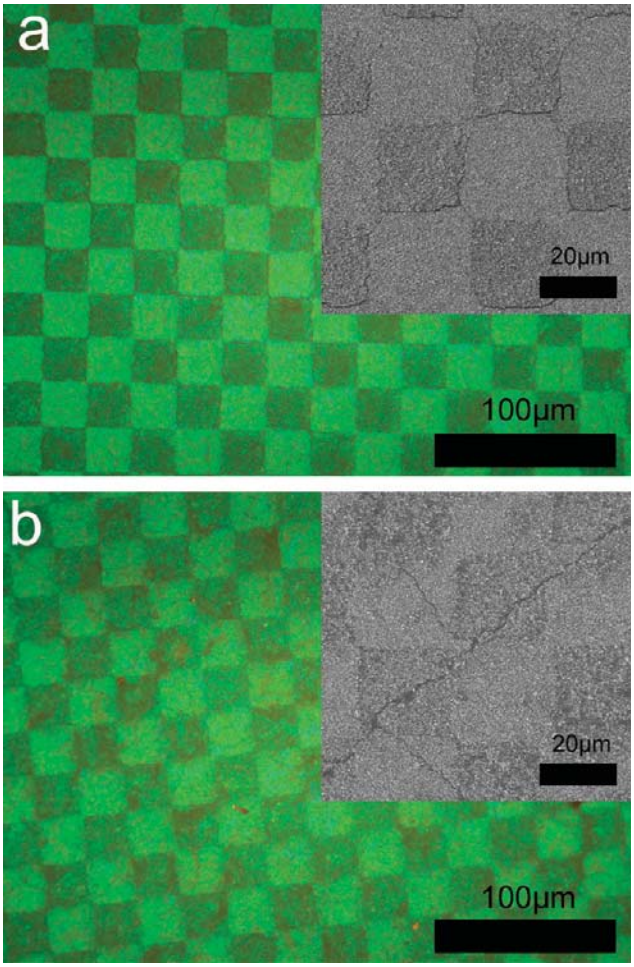

Figure 5. Comparative images illustrating that (a) the annealing process (60 °C) applied to the samples benefitted the patterning cracks and (b) simply breaking apart the two substrates did not lead to good crack patterns.

to the calculated one (509 nm) if using 230 nm as D. This kind of slight red shift might originate from the remnant solvent trapped in the voids, which increases the n_{vo} or some nonclosely packed areas that increase the d_{111}.

Note that the annealing process was necessary to obtain designed crack patterns because it was not simply heating[34] or melting[35] the CC to reduce defects or faults but rather was a process aimed at letting the CC system undergo and then pass the "transition state",[36] a state in which the spheres have already formed the fcc structure but still maintain some mobility with the presence of the remnant solvent. Our annealing process began with filling the CC with water to ensure that it could definitely reach this state, and then we heated it to remove the solvent (highest temperature, 100 °C, which prevented water from boiling), causing an abrupt transition and exerting shock stresses on the crystal.[36,37] As a result, cracks were inevitably formed because of much severer capillary stress and shrinkage of the spheres upon drying, allowing the template to make a difference during this process, which will be addressed in the section Mechanism for Template Recognition. As shown in Figure 5b, if we remove the top substrate before annealing, then the regular crack patterns due to template recognition were almost lost,

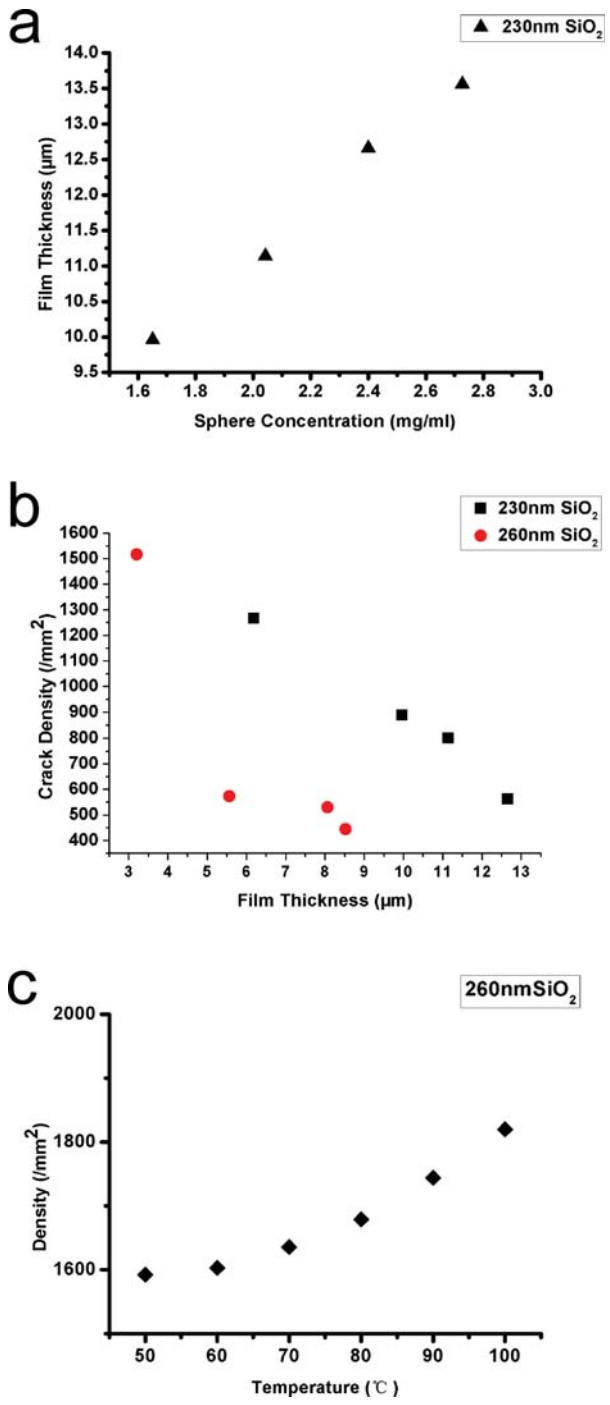

Figure 6. (a) Film thickness as a function of the concentration of the spheres used during self-assembly at room temperature (sphere size, ~230 nm; template pattern, squares). (b) Crack density as a function of film thickness and as influenced by the sphere size (annealing temperature, 70 °C; template pattern, squares). (c) Crack density versus annealing temperature applied to 3.21 μm CC films formed by 260 nm spheres (template pattern, squares and triangles). Note that the tendency resembles an increasing function. (The samples were quickly cooled to room temperature after heating.)

resembling the complementary patterns in Parikh's method, in which square islands that consisted of a few layers of spheres existed on one substrate and grid walls with the same thickness were left on the other substrate. In our method, on the Si template substrate, spheres existed only on hydrophilic regions, likewise demonstrating the stickiness contrast, shown in Figure 3a, whereas on the glass substrate, the spheres formed a bulk colloidal crystal that covered the whole area, also displaying the corresponding pattern shown in the SEM images in Figure 2c,f,i and in the inset image of Figure 5a. However, Figure 3b shows that the residual silica spheres in hydrophilic regions on the template substrate did not exhibit planar surfaces such as the ones reported by Parikh's group. Instead, we obtained only one layer of spheres in these regions on the template, with a few more spheres stuck above this layer, appearing as a rough surface. We presume that the cleavage from the substrates preferentially occurred at the hydrophobic substrate surfaces but not at the hydrophilic surfaces because stickiness existed between the spheres and the hydrophilic substrates to bind the two kinds of materials together, though not too tightly. Compared with their work, our CC films are thicker and the scales of the single-crystal domains are much smaller, wherein no further cracks exist. (The element figures' diameters or side lengths are equal to or less than 50 μm.) Moreover, the cracks along the borderlines in our system do not result from the opening-up operation, which is the cause of the cleaved edges of the domains in their excellent CC arrays, even though both groups used template recognition. When splitting the two substrates with a scalpel, cleavages started at the breakable planes whereby delamination[38] might have already occurred, leaving one or two layers of spheres stuck on the hydrophilic regions of the template substrate, resulting in the alternate planar/rough topographies. It is also worth mentioning that if the two substrates were both hydrophilic (i.e., no template was used when preparing the 3D CC) then the resulting sample would lose both the crack pattern and the roughness pattern. An example is given in the Supporting Information as Figure S3, which resembles the common CC prepared in other work.

Crack Density. An evident difference is shown in Figure 5a (annealed) and Figure 5b (not annealed) in that the annealing process increased the density and the visibility of the secondary cracks. In addition, the cracks propagated along the hydrophilic/hydrophobic boundaries because of the discrepancy brought about by the substrate inducement during the shrinkage process. We pictured the surfaces of the CCs and measured the number of cracking points per unit visualization area (i.e., the crack density) following Yamamura's method[31] in which three kinds of densities according to connecting situations are defined: PN (the number of points at which an isolated primary crack nucleates), SN (the number of points at which a secondary crack nucleates from an existing crack), and CN (the number of points at which a propagating crack connects or merges with a neighboring one). In our work, we calculated the total density (PN + SN + CN = total connecting points/photographic area) for convenience. According to the mechanism and laws proposed by Lee et al.,[39] the crack spacing is largely concerned with capillary stress. In their system, the spacing scales with the film thickness to the power of 0.8, the evaporation rate scales to the power of −0.35, and the particle size scales to the power of 0.2. In this regard, we adjusted the total density of all kinds of cracks, which relieve the lateral stress of the colloidal crystal film, as shown in Figure 6a,b, mainly by altering the concentration of the colloidal suspensions to form different film thicknesses while using fixed sphere sizes during deposition and fixed annealing temperatures (the evaporation rate scales with temperature[40]). It appears that the film

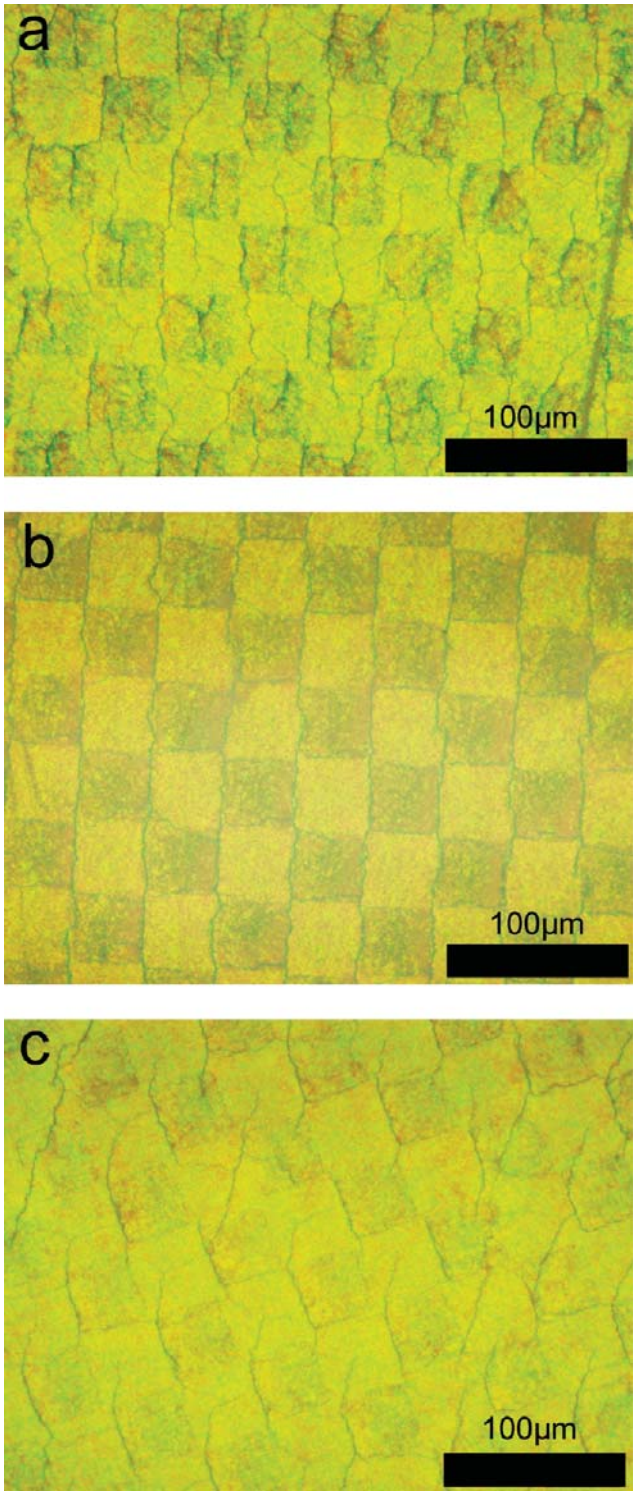

Figure 7. (a−c) Optical photographs of the cracks with different densities in the patterned CCs formed by 260 nm SiO_2 spheres (high density, 1192 mm^{-2}; thickness, 3.7 μm; annealed at 50 °C; appropriate density, 867 mm^{-2}; thickness, 4.8 μm; annealed at 50 °C; low density, 552 mm^{-2}; thickness, 5.5 μm; annealed at 70 °C, respectively). The length of the squares is 45 μm.

thickness simply scales with the sphere concentration, exhibiting a linear relationship, as long as there are enough spheres to fill in the interstice between the two substrates. As to the crack density, it decreases as the CC film becomes thicker, almost linearly scaling with the film thickness (when the annealing temperature and sphere size are fixed at 70 °C and 230 nm/260 nm). Additionally, the less critical factors (sphere size and annealing temperature) that affect the crack density were also investigated with simple trials, which could also provide support for the adjustment of the crack density. As depicted in Figure 6b,c, using larger spheres can lead to fewer cracks (when the annealing temperature and film thickness are fixed at 70 °C and a certain thickness), and the crack density increases slowly from 1600 to 1800 mm^{-1} as the annealing temperature ranges from 50 to 100 °C (when the sphere size and film thickness are fixed at 230 nm and 3.21 μm, respectively). The results generally correspond to the tendencies in Lee's report if we assume that the crack density simply increases as the mean crack spacing decreases. It is also worth noting that the data concerning cracks sometimes appear as a great deviation around the presumed trend line, which is often the case in other reports that we mentioned, so here we used only data points that are concise and representative but all of the data shown in Figure 6 were obtained from the samples prepared with templates.

Although Lee focused his work on investigating the main cracks, it seems that the total crack density is also affected by the factors that he proposed. Because we do not aim to simulate the cracking process, the detailed proposed mechanisms and modeling discussions are not included in this article. As to the density's influence on the pattern quality, Figure 7a−c (crack densities of 1192, 867, 552 mm^{-2}, respectively) shows that when there are too many or too few cracks, only some of them can still be located in the predominant lines (the square borderlines). Other cracks prefer to maintain their intrinsic spacing order regarding the template inducement as a weak factor of their forming location. Therefore, an appropriate crack density is important in manipulating cracks, which can ensure that the number of connecting crack points is nearly equal to the number of intersecting points of the template pattern. Interestingly, when the crack density is not lower than half of the appropriate value, regular patterns are also formed depending on the template design. For example, a rhombus CC array was obtained using a template with the pattern of a triangle array (Figure 2g−i). If one edge shared by two neighboring triangles is not dominated by cracks, then two triangles will turn into a rhombus, but sometimes a propagating crack was attracted by two neighboring edges on its way so this kind of dilemma resulted in pattern faults (a crack took up the wrong edge or did not dominate either edge). We also found that when we employed circles that were separated from each other as the template pattern, the cracks went through the barriers and preferred to form hexagonal units with shared edges rather than separate circles (maybe because the cracks tend to connect to each other and propagate straightly as they usually do), exhibiting their behavior of not only generating enough cracking points but also accepting template inducement (Figure 2d−f). Note that the annealing process should be applied soon after the CC film has been formed; otherwise, cracks that are wide and far away from each other would gradually spread over the CC film at room temperature and relieve the stress to an great extent, which makes it difficult to control the crack density and position further .

Mechanism for Template Recognition. Usually, the crack patterns observed under natural conditions are irregular, like those in paintings and on drought-prone land, whereas the crack spacing distribution could be narrow and the density could be certain in undisturbed systems. The relevant mechanism concerns the

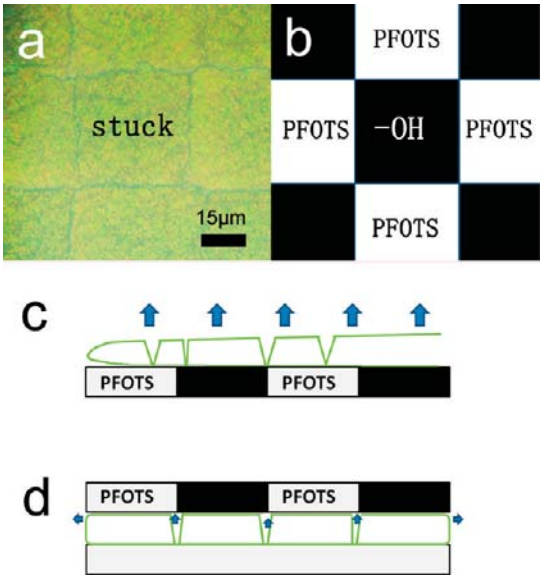

Figure 8. (a) Fracture mechanism illustrated in an optical image of the chessboard-like colloidal crystal array using spheres with a diameter of ~260 nm. (b) Illustration of the surface chemical groups of the template. (c) Schematic of the cracking processes of employing only a single template substrate, which cannot generate nicely regular patterns. (d) Schematic of the cracking processes of employing two substrates.

elimination of capillary pressure due to the yielding of the material, and the pressure gradient has already been described in some papers.[40,41] Once the crack density fits the periodicity of the template pattern, we can further regulate the path of the cracks by bringing in a surface energy discrepancy. The dark square in the center of Figure 8a was originally against a black square with −OHs on the surface in Figure 8b before breaking apart the two substrates, and the bright squares were against the black squares covered with PFOTS. In this case, water in the hydrophobic regions was repelled during annealing, creating the borderlines of the distribution of capillary stress. At the same time, the annealing and cooling process made the shrinkage severe enough to let the stickiness discrepancy work. Specifically, because the spheres were glued to the hydrophilic regions of the patterned substrate, they would be constrained by the surface to some extent and would not be easily dragged away by those around them when they underwent severe shrinkage. We believe that both of these two factors resulted that the spheres parallel to the hydrophilic regions and those parallel to the hydrophobic regions shrank separately as two kinds of groups, and the cracks preferred to be generated at the borderlines of the two kinds of regions. In addition, we have found that the patterned template has little effect when annealed without another substrate, which is because the outer layers of the CC are in direct contact with the atmosphere, leading to an inhomogeneous distribution of solvent that causes the outer layers to be dried easily and to form the starting points of cracks. Therefore, the formation of cracks in this case cannot be directly affected by the template inducement, as depicted in Figure 8c, which resembles the illustration in Hull and Caddock's paper.[38] However, when annealing the sandwich we described (Figure 8d) instead of the system including only one substrate, the CC will undergo a much slower drying process, during which most of the water vapor has to go out through the cracks connecting to the outer atmosphere. Once the cracks start

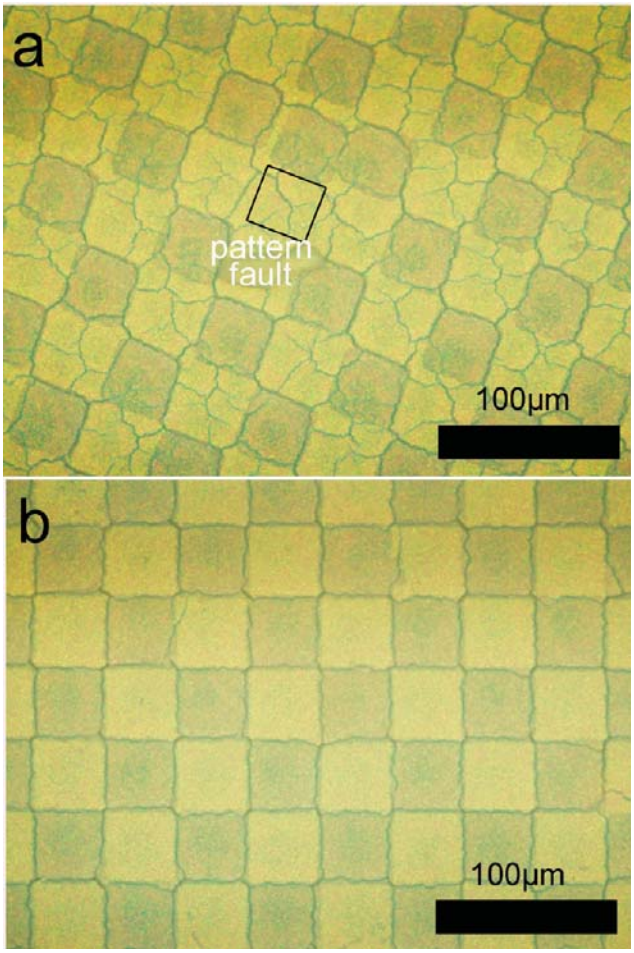

Figure 9. Optical photographs of the cracks with (a) a high density and (b) an appropriate density formed in the PVP-doped CCs after annealing and short-time calcination at 450 °C.

to form at the borderlines that we designed, they then propagate, with physical protection in place to allow the template inducement to take place and to let the vapor flow away through their channel-like paths.

By trying to reduce the random cracks that ignore the template inducement during severe and fast shrinkage, we added a little PVP to the colloidal suspension to increase the viscosity between the spheres so that they shrank together to increase the robustness of the CC film against capillarity upon drying.[42] The resulting crack patterns after annealing and calcination are shown in Figure 9a,b. Though the packing quality is not perfect judging from the reflective color (SEM image available in Supporting Information Figure S4), the discrepancies brought about by the template appears to be more significant because we could see that all of the borderlines were dominated by cracks. Moreover, when the crack density was above the appropriate value, we found that the number of extra cracks in the bright domains exceeded the number of them in the dark ones (Figure 9a), which were previously against the hydrophilic regions of the template. This illustrates that the stress prefers to be relieved at these places after the borderlines have already been dominated by the induced cracks. It appears that when the cracks were trying to go into the dark squares, they were "shielded"; therefore, the cracks propagated along the "shield" borderlines or even branch, just the way a

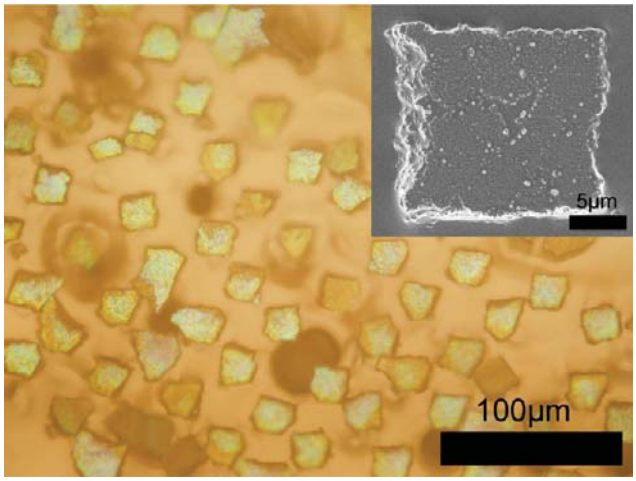

Figure 10. Optical photograph of single CCs detached from the substrate. The inset is an SEM image showing the square shape.

river does when it encounters a large rock in its path. Moreover, the crack situations change between the two neighboring squares at the pattern fault in Figure 9a. The result substantiates the hypothesis that the shrinkage of the silica spheres was much more restrained against the hydrophilic regions of the template, compared to the spheres against the hydrophobic regions. However, the template acts more as an inducer rather than a crack density adjuster. Cracks will actually propagate only if this propagation reduces the total energy,[23] including elastic and crack energy. For such a dissipative structure, a severe interruption will produce an increase in the total energy of the system, which is not preferred, and this is why the crack density should fit the periodicity of the template pattern to obtain the best results.

Single Colloidal Crystals Detached from the Substrates. Furthermore, to confirm that these single crystals are truly separated from each other, we have attempted to detach such small crystals from the substrate. We believe that such colloidal crystals on the micrometer scale have the potential to be supports for quantum dots[43] and bioassay.[44] Because the CC islands will easily break without calcination, we first heated the samples to a lower temperature (450 °C) to allow the spheres to shrink even more severely and then to a higher temperature (700 °C) to increase the mechanical strength. Note that the samples could not be calcinated at high temperature for too long (more than 2 h) because the substrate would melt and stick tightly to the CCs, hindering detachment. In Figure 10, a number of small crystal cakes that detached from the calcinated substrate preserve the square shape and photonic properties (whereas some were still damaged during detachment). As demonstrated in the inset of Figure 10, the spheres pack in an fcc structure and the crystals are thicker than just a few layers (23 layers for the CC in this image). Such 3D CCs with a designed shape and size were seldom seen in other patterning techniques, which usually obtained balls[45] or hemispheres.[46] (Another kind of micro-CC with the shape of a hexagon was also obtained, as shown in Supporting Information Figure S5).

CONCLUSIONS

We have observed and investigated the cracking behavior of the colloidal crystals confined in a sandwich-like device, which possesses a surface energy pattern template that directly affects the shrinkage of the CC film. By applying annealing and calcination, we manipulated the cracks to cleave the 3D colloidal crystal thick film into various kinds of single-crystal blocks on the subhundred micrometer scale. This process does not need refined techniques such as e-beam lithography to incise the matter line by line from the outside but possesses the intrinsic behavior of stress relief. Moreover, this economic method allows mass production, assuring the high uniformity of the crystal structure properties and a high ratio of space utilization for the reason that the single crystals preserve the parent crystal's structural order and the interstices between them are cracks with the width of merely one or several spheres' diameter. More work will be carried out on applying the method to other sol−gel systems as well as obtaining inverse-opal structures with certain shapes.

ASSOCIATED CONTENT

Supporting Information. Photoresist patterns, close-up image of the sphere packing on both sides of a linear crack, photograph of the common CC prepared with no template, and SEM images of a PVP-doped CC and a micro-CC in the shape of hexagon. This material is available free of charge via the Internet at http://pubs.acs.org.

AUTHOR INFORMATION

Corresponding Author
*E-mail: zjh@jlu.edu.cn.

ACKNOWLEDGMENT

This work was supported by the National Natural Science Foundation of China (grant nos. 21074048, 20921003, and 20874039) and the National Basic Research Program of China (2007CB936402).

REFERENCES

(1) Ozin, G. A. *Chem. Commun.* **2003**, *21*, 2639–2643.
(2) Xia, Y.; Gates, B.; Yin, Y.; Lu, Y. *Adv. Mater.* **2000**, *12*, 693–713.
(3) Meseguer, F. *Colloids Surf., A* **2005**, *270*, 1–7.
(4) Jiang, P.; Bertone, J. F.; Hwang, K. S.; Colvin, V. L. *Chem. Mater.* **1999**, *11*, 2132–2140.
(5) Miguez, H.; Meseguer, F.; Lopez, C.; Blanco, A.; Moya, J. S.; Requena, J.; Mifsud, A.; Fornes, V. *Adv. Mater.* **1998**, *10*, 480–483.
(6) Yao, J. M; Yan, X.; Lu, G.; Zhang, K.; Chen, X.; Jiang, L.; Yang, B. *Adv. Mater.* **2004**, *16*, 81–84.
(7) Li, T.; Xing, R. B.; Huang, W. H.; Han, Y. C. *Colloids Surf., A* **2005**, *269*, 22–27.
(8) Zhao, Y. J.; Zhao, X. W.; Sun, C.; Li, J.; Zhu, R.; Gu., Z. Z. *Anal. Chem.* **2008**, *80*, 1598–1605.
(9) Xu, L.; Li, H.; Jiang, X.; Wang, J. X.; Li, L.; Song, Y. L.; Jiang, L. *Macromol. Rapid Commun.* **2010**, *31*, 1422–1426.
(10) Fernandes, G. E.; Beltran-Villegas, D. J.; Bevan, M. A. *J. Chem. Phys.* **2009**, *131*, 134705.
(11) Okubo, T.; Nakagawa, N.; Tsuchida, A. *Colloid Polym. Sci.* **2007**, *285*, 1247–1255.
(12) Kubo, S; Gu, Z. Z.; Tryk, D. A.; Ohko, Y; Sato, O; Fujishima, A. *Langmuir* **2002**, *18*, 5043–5046.
(13) Kuncicky, D. M.; Prevo, B. G.; Velev, O. D. *J. Mater. Chem.* **2006**, *16*, 1207–1211.
(14) Lu, L. H.; Eychmüller, A. *Acc. Chem. Res.* **2008**, *41*, 244–253.
(15) Yang, L.; Kang, J.; Guan, Y.; Wei, F.; Bai, S.; Zhang, M.; Zhang, Z.; Cao, W. *Langmuir* **2006**, *22*, 11275–11278.

(16) Sun, Z. Q.; Li, Y.; Zhang, J. H.; Li, Y. F.; Zhao, Z. H.; Zhang, K.; Zhang, G.; Guo, J. R.; Yang, B. *Adv. Funct. Mater.* **2008**, *18*, 4036–4042.
(17) Li, F.; Wang, Z.; Stein, A. *Angew. Chem., Int. Ed.* **2007**, *46*, 1885–1888.
(18) Li, M. Z.; He, F.; Liao, Q.; Liu, J.; Xu, L.; Jiang, L.; Song, Y. L.; Wang, S.; Zhu, D. B. *Angew. Chem., Int. Ed.* **2008**, *47*, 7258–7262.
(19) Li, H.; Wang, J. X.; Lin, H.; Xu, L.; Xu, W.; Wang, R. M.; Song, Y. L.; Zhu, D. B. *Adv. Mater.* **2010**, *22*, 1237–1241.
(20) Kanai, T.; Sawada, T. *Langmuir* **2009**, *25*, 13315–13317.
(21) Wang, L.; Zhao, X. S. *J. Phys. Chem. C* **2007**, *111*, 8538–8542.
(22) Chen, X.; Chen, Z. M.; Yang, B; Zhang, G.; Shen, J. C. *J. Colloid Interface Sci.* **2004**, *269*, 79–83.
(23) Hofmann, M.; Bahr, H. A.; Linse, T.; Bahr, U.; Balke, H.; Weiss, H. F. *Int. J. Fract.* **2006**, *141*, 345–356.
(24) Dufresne, E. R.; Corwin, E. I.; Greenblatt, N. A.; Ashmore, J.; Wang, D. Y.; Dinsmore, A. D.; Cheng, J. X.; Xie, X. S.; Hutchinson, J. W.; Weitz, D. A. *Phys. Rev. Lett.* **2003**, *91*, 224501.
(25) Griesebock, B.; Egen, M.; Zentel, R. *Chem. Mater.* **2002**, *14*, 4023–4025.
(26) Chen, X.; Sun, Z. Q.; Chen, Z. M.; Shang, U.; Zhang, K.; Yang, B. *Colloid Surf., A* **2008**, *315*, 89–97.
(27) Koh, Y. K.; Wong, C. C. *Langmuir* **2006**, *22*, 897–900.
(28) Stöber, W.; Fink, A.; Bohn, E. *J. Colloid Interface Sci.* **1968**, *26*, 62–69.
(29) Zhao, Q; Zheng, J. M.; Chai, B. H.; Pollack, G. H. *Langmuir* **2008**, *24*, 1750–1755.
(30) Dufresne, E. R.; Corwin, E. I.; Greenblatt, N. A.; Ashmore, J.; Wang, D. Y.; Dinsmore, A. D.; Cheng, J. X.; Xie, X. S.; Hutchinson, J. W.; Weitz, D. A. *Phys. Rev. Lett.* **2003**, *91*, 224501.
(31) Yamamura, M.; Ono, H.; Uchinomiya, T.; Mawatari, Y.; Kage, H. *Colloids Surf., A* **2009**, *342*, 65–69.
(32) Brozell, A. M.; Muha, M. A.; Parikh, A. N. *Langmuir* **2005**, *21*, 11588–11591.
(33) Maka, T.; Chigrin, D. N.; Romanov, S. G.; Sotomayor Torres, C. M. *Prog. Electron. Res. PIER* **2003**, *41*, 307.
(34) Ma, X. Y.; Li, B. J.; Chaudhari, B. S. *Appl. Surf. Sci.* **2007**, *253*, 3933–3936.
(35) Harada, M.; Ishii, M.; Nakamura, H. *Colloids Surf., B* **2007**, *56*, 220–223.
(36) Koh, Y. K.; Teh, L. K.; Wong, C. C. *Thin Solid Films* **2008**, *516*, 5637–5639.
(37) Koh, Y. K.; Wong, C. C. *Langmuir* **2006**, *22*, 897–900.
(38) Hull, D.; Caddock, B. D. *J. Mater. Sci.* **1999**, *34*, 5707–5720.
(39) Lee, W. P.; Routh, A. F. *Langmuir* **2004**, *20*, 9885–9888.
(40) Lee, W. P.; Routh, A. F. *Ind. Eng. Chem. Res.* **2006**, *45*, 6996–7001.
(41) Scherer, G. W. *J. Non-Cryst. Solids* **1992**, *144*, 210–216.
(42) Choi, H. K.; Kim, M. H.; Im, S. H.; Park, O. O. *Adv. Funct. Mater.* **2009**, *19*, 1594–1600.
(43) Li, J.; Zhao, X. W.; Zhao, Y. J.; Gu, Z. Z. *Chem. Commun.* **2009**, 2329–2331.
(44) Sun, C.; Zhao, X. W.; Zhao, Y. J.; Zhu, R.; Gu, Z. Z. *Small* **2008**, *4*, 592–596.
(45) Cho, Y. S.; Kim, S. H; Yi, G. R.; Yang, S. M. *Colloids Surf., A* **2009**, *345*, 237–245.
(46) Kim, S. H.; Lim, J. M.; Jeong, W. C.; Choi, D. G.; Yang, S. M. *Adv. Mater.* **2008**, *20*, 3211–3217.